Unexpected magnetism, Griffiths phase, and exchange bias in the mixed lanthanide $Pr_{0.6}Er_{0.4}Al_2$

Arjun K. Pathak,[1,*] D. Paudyal,[1] W. T. Jayasekara,[1,2] S. Calder,[3] A. Kreyssig,[1,2] A. I. Goldman,[1,2]
K. A. Gschneidner, Jr.,[1,4] and V. K. Pecharsky[1,4]

[1]*The Ames Laboratory, U.S. Department of Energy, Iowa State University, Ames, Iowa 50011, USA*

[2]*Department of Physics and Astronomy, Iowa State University, Ames, Iowa 50011, USA*

[3]*Quantum Condensed Matter Division, Neutron Sciences Directorate, Oak Ridge National Laboratory, Oak Ridge, Tennessee 37831, USA*

[4]*Department of Materials Science and Engineering, Iowa State University, Ames, Iowa 50011, USA*

(Received 18 February 2014; revised manuscript received 29 May 2014; published 17 June 2014)

We report an unusual coexistence of ferromagnetism and ferrimagnetism, and metamagnetism in $Pr_{0.6}Er_{0.4}Al_2$. In addition, this compound retains a clear Griffiths phase behavior even at 1 kOe magnetic field and shows a large exchange bias after field cooling from the paramagnetic state. The crystal-field excitations and opposite exchange interactions between nearest-neighbor and next-nearest-neighbor rare earth sites explain these behaviors.

DOI: 10.1103/PhysRevB.89.224411 PACS number(s): 71.20.Eh, 61.50.Ks, 65.40.Ba

I. INTRODUCTION

The coexistence of different magnetic functionalities, such as Griffiths phase [1], ferromagnetic (FM) and ferrimagnetic (FIM) states [2], and field-induced first-order metamagnetic transitions in a single compound [3], is important for both fundamental science and practical applications. In particular, the Griffiths phase is an unusual magnetic state characterized by nonlinearity of inverse magnetic susceptibility in the nominally paramagnetic (PM) phase, where magnetic clusters of finite size exist [4,5]. Diluted Ising ferromagnets [6] and colossal magnetoresistance materials [7] are two common examples of materials that exhibit the Griffiths phase.

Similar to magnetic inhomogeneities in the PM phase, competition between FM and antiferromagnetic (AFM) or FIM phases creates superb interest within the scientific community, and its importance has been revealed, for example, in spintronic devices such as spin valves, read heads, and nonvolatile memory [8]. Quite often, cooling such a system in nonzero magnetic fields starting from temperatures above the magnetic ordering displaces the hysteresis loop, $M(H)$, making it asymmetrical with respect to the origin of coordinates of the M-H coordinate system. Asymmetry of hysteresis, or exchange bias (EB), is attributed to exchange interactions between the AFM or FIM and field-induced FM phases and is usually observed in thin films and multilayered magnetic systems [9], being a rare occurrence in bulk materials [10,11].

Rare earth dialuminides, RAl_2, have been broadly studied in the past, revealing interesting physics, such as strong crystal-field (CF) effects, due to anisotropic $4f$ charge density and anomalous low-temperature (LT) magnetic and crystal structures [12,13]. Combining *two heavy* lanthanides in $R_{1-x}R'_xAl_2$ leads to additional magnetic reordering transitions below their respective T_C that may appear and vanish with x [14]. Despite a long history of research on rare earth dialuminides, mixed *light and heavy* lanthanide compounds have been scarcely studied, keeping potentially interesting physics unexposed. In particular, mixed light and heavy lanthanide dialuminides, $R_{1-x}R'_xAl_2$, where the geometry of $4f$ charge densities of R is different from R' (i.e., prolate vs oblate spheroids), represent an interesting choice for studies since the spin-orbit coupling constants for light and heavy lanthanides are opposite to each other, and competition between such magnetic ions can lead to anomalous physics. Interesting effects have been reported [15–17], but the science of such materials is far from being understood and complete.

Here we report unusual physical properties, including a large EB, short-range FM, FIM, and first-order magnetic field induced transitions in $Pr_{0.6}Er_{0.4}Al_2$. To the best of our knowledge, none of the dialuminides formed by either the individual lanthanides or their mixtures have been reported to exhibit such a peculiar combination of multiple physical phenomena in a single compound. The observed magnetic states and physical behaviors are interpreted using density functional theory (DFT) calculations.

II. EXPERIMENTAL AND COMPUTATIONAL DETAILS

Polycrystalline $Pr_{1-x}Er_xAl_2$ samples with $0 \leqslant x \leqslant 0.95$ were prepared by arc melting stoichiometric amounts of the constituent elements in an argon atmosphere. In this paper, we focus on the alloy with $x = 0.4$, which has distinctly anomalous physical behaviors among other prepared alloys; i.e., it is the only composition that exhibits a clear temperature hysteresis between magnetization measured on cooling and warming that develops with increasing magnetic field. The Pr and Er metals were obtained from the Materials Preparation Center of the Ames Laboratory and were, respectively, 99.98+ wt% (99.85+ at.%) and 99.98+ wt% (99.82+ at.%) pure with respect to all other elements in the periodic table [18]. The Al metal of 4N purity was purchased from Alfa Aeser. The crystal structure was determined by powder x-ray diffraction (XRD) experiments performed at temperatures ranging between room temperature and 5 K in zero and applied magnetic fields up to 40 kOe using the x-ray powder diffractometer described by Holm *et al.* [19]. The structural parameters were determined by Rietveld analysis using LHPM Rietica [20]. The dc magnetization was measured in a Quantum Design superconducting quantum interference device (MPMS-XL7 magnetometer) and a Physical Property Measurement System (PPMS) by using the vibrating sample magnetometer at magnetic fields up to 140 kOe. The heat capacity measurements were performed

*Corresponding author: pathak138@ameslab.gov

 ©2014 American Physical Society

using a homemade adiabatic heat-pulse calorimeter [21] at applied magnetic fields up to 100 kOe.

Neutron powder diffraction measurements on a 4 g sample of $(Pr_{1-x}Er_x)Al_2$ ($x = 0.4$) were carried out using the HB2A neutron powder diffractometer [22] at the High Flux Isotope Reactor at Oak Ridge National Laboratory, using a wavelength of $\lambda = 2.4065$ Å provided by a vertically focusing Ge(113) monochromator. Collimators with divergencies of 12′–21′–6′ were located before the monochromator, between the monochromator and sample, and between the sample and detectors, respectively. The sample was held in a cylindrical vanadium container in a top-loading closed-cycle refrigerator (4–300 K). Powder patterns were collected above ($T = 40$ K) and below (T = 5 K) the ordering temperature of $Pr_{0.6}Er_{0.4}Al_2$ ($T_C = 24$ K). Rietveld refinements of the powder data were performed using FULLPROF [23].

Density functional theory (DFT) calculations were performed using the local spin density approximation with the Hubbard U (LSDA + U) approach [24] within tight binding linear muffin tin orbital (TB-LMTO) [25] and full potential linear augmented plane wave (FPLAPW) [26] methods. The LSDA + U approach takes into account orbital dependency of U and J. Values of $U = 6.7$ eV and $J = 0.7$ eV, which are well known for Gd, were used to model strong electron-electron correlations for Er and Pr atoms. The calculations for $Pr_{0.625}Er_{0.375}Al_2$ (which is close to the experimentally studied $Pr_{0.6}Er_{0.4}Al_2$) were performed by changing the cubic symmetry to $P1$ symmetry and randomly placing five Pr and three Er atoms in the eight rare earth positions in a formally triclinic unit cell with $a = b = c$ and $\alpha = \beta = \gamma = 90°$ that has the same unit cell volume as the cubic unit cell. Because of the localized nature of the $4f$ electrons, different random placements of five Pr and three Er atoms in 56 possible combinations show identical local $4f$ CF splitting and the local magnetic moments. This indicates that the actual placement of Pr and Er atoms in the pseudocubic triclinic unit cell has little to no effect on the calculated magnetic properties of $Pr_{0.625}Er_{0.375}Al_2$, assuming collinear magnetism between Pr and Er atoms.

III. RESULTS AND DISCUSSION

The dc magnetization, $M(T)$, of $Pr_{0.6}Er_{0.4}Al_2$ measured as a function of temperature at various magnetic fields is shown in Fig. 1. Zero field cooled (ZFC) warming, field cooled cooling (FCC), and field cooled warming (FCW) $M(T)$ values show a small kink in the magnetization curves around 24 K at $H = 10$ kOe [Fig. 1(a)]. The temperature at which the kink is observed decreases, and the kink itself (i.e., the discontinuity in the magnetization at that temperature) becomes more prominent with increasing magnetic field [Figs. 1(a)–1(d)]. The anomaly finally disappears with the application of magnetic field of 100 kOe [Fig. 1(e)]. The thermal hysteresis between FCC and FCW $M(T)$ data gradually increases with increasing applied magnetic field, is most noticeable for $H = 70$ kOe [Fig. 1(d)], and disappears when $H \geqslant 100$ kOe [Fig. 1(e)].

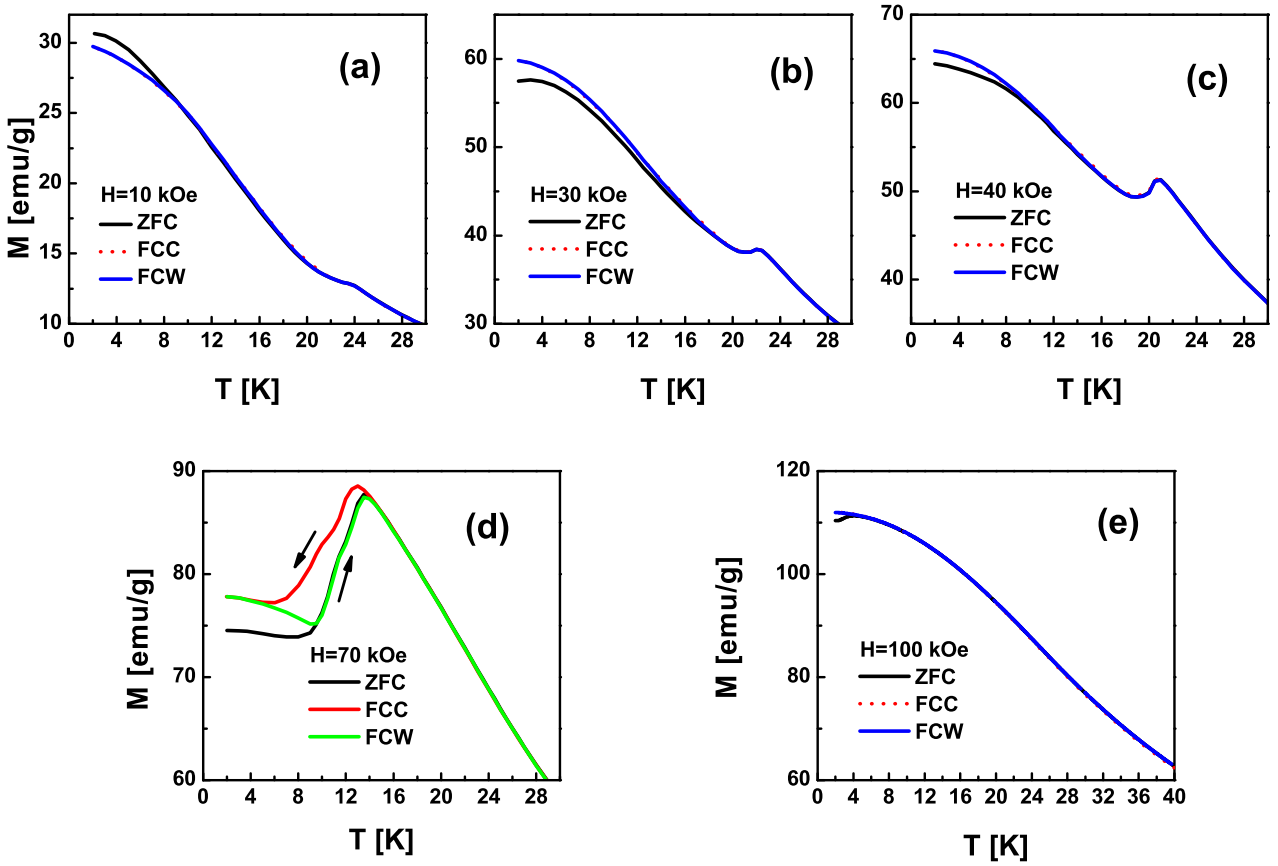

FIG. 1. (Color online) (a–e) Zero field cooled warming, field cooled cooling, and field cooled warming magnetization of $Pr_{0.6}Er_{0.4}Al_2$ measured at various magnetic fields.

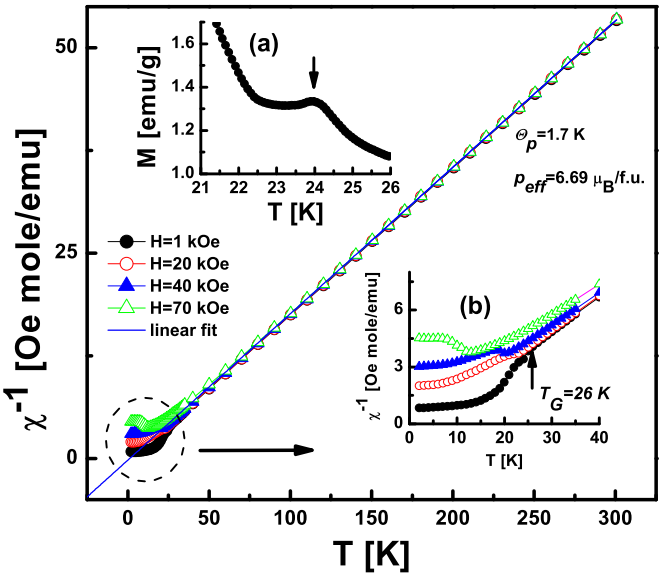

FIG. 2. (Color online) The inverse dc magnetic susceptibility χ^{-1} (H/M) measured as a function of temperature at various magnetic fields. The insets (a) and (b) show details of magnetization as a function of temperature at $H = 1$ kOe and the low-temperature χ^{-1} behavior at various magnetic fields, respectively.

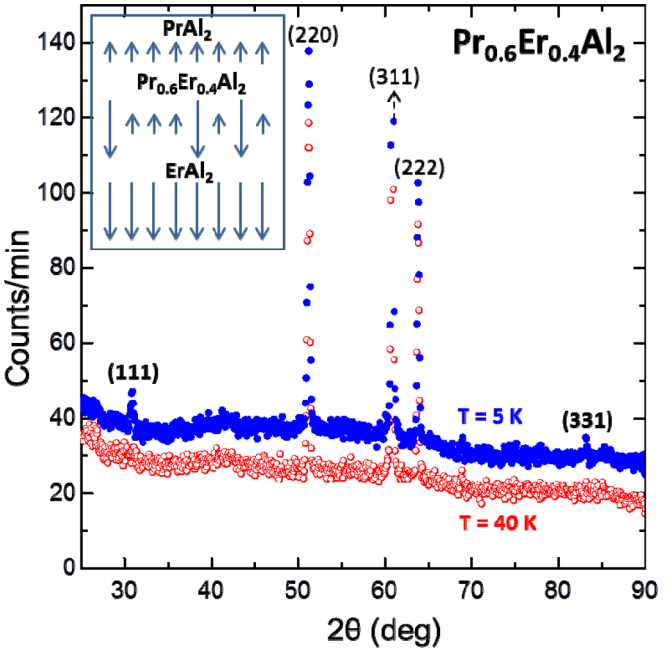

FIG. 3. (Color online) Neutron powder patterns at $T = 40$ K and 5 K. The additional magnetic scattering at the chemical Bragg peak positions is most clearly seen for the (111) and (331) reflections. The inset shows a schematic of the antiparallel orientations of the Pr and Er moments below the ferrimagnetic transition at 24 K.

The inverse dc magnetic susceptibility ($\chi^{-1} = H/M$) of $Pr_{0.6}Er_{0.4}Al_2$ measured in magnetic fields up to 70 kOe is presented in Fig. 2. At $H = 1$ kOe, χ^{-1} shows two distinct temperature-dependent regimes: at high temperatures (>50 K), it exhibits a typical Curie-Weiss behavior; at low temperatures, a sharp downturn is observed below a characteristic temperature, the Griffiths temperature T_G, signaling the onset of a Griffiths phase, which is characterized by short-range FM clustering due to competing interactions between Pr and Er atoms (inset b, Fig. 2). Similar behavior has also been observed in other localized $4f$ systems [5] and itinerant magnetic semiconductors [27], but only at very low applied fields ($0 \leqslant H \leqslant 20$ Oe). Upon an increase of the magnetic field from 1 kOe to $H \geqslant 20$ kOe, the negative deviation of χ^{-1} vanishes, the absolute value of χ^{-1} increases with increasing magnetic field, and field-dependent steplike anomalies emerge, indicating field-induced phase transitions (inset b, Fig. 2). $M(T)$ values measured in $H = 1$ kOe (inset a, Fig. 2) suggest that $Pr_{0.6}Er_{0.4}Al_2$ undergoes a PM to FIM-like transition at $T_C = 24$ K. The effective moment, p_{eff}, and the Weiss temperature, Θ_{pm}, calculated using $H = 70$ kOe data are 6.69 μ_B and 1.7 K, respectively. The observed p_{eff} is in excellent agreement with the expected value of 6.69 μ_B for 0.6Pr+0.4Er and is consistent with the Er and Pr atoms randomly occupying the same site. The random distribution of Er and Pr atoms on the same site is not surprising given the chemical similarity and the small size difference of the lanthanides, and it is found in all mixed lanthanide compounds [17,28,29]. Proximity of Θ_{pm} to 0 K supports the argument that FIM interactions are strong, if not dominant.

Neutron powder patterns at $T = 40$ K and 5 K are shown in Fig. 3. At $T = 40$ K (zero magnetic field), the neutron powder diffraction pattern of $Pr_{0.6}Er_{0.4}Al_2$ only displays Bragg peaks consistent with the $MgCu_2$-type chemical structure. The FULLPROF refinement ($R_{wp} = 5.65\%$) confirms the nominal stoichiometry, $Pr_{0.60\pm0.01}Er_{0.40\pm0.01}Al_2$, yields the lattice parameter $a = 7.9212(1)$ Å, and is consistent with a random distribution of Pr and Er atoms occupying a single available rare earth site. At $T = 5$ K (below $T_C = 24$ K), additional scattering is observed only at nuclear reflections, most notably at (111) and (331) Bragg peaks. Assuming that both Pr and Er participate in the long-range magnetic order, refinement of the magnetic structure [FULLPROF, R_{wp}(mag) = 13.2%] is consistent with FIM ordering of the Pr and Er moments along the [100] direction (see inset in Fig. 3) with an average moment of 0.9(2) μ_B/R. This is somewhat smaller than 1.55 μ_B [30] expected for the antiparallel arrangement of Pr and Er moments randomly distributed on the rare earth sites, but not unreasonably so.

The ZFC isothermal magnetization $M(H)$ at $T = 2$ K [Fig. 4(a)] shows FIM-like behavior up to $H \cong 65$ kOe and then reveals several consecutive metamagnetic transitions between 70 and 115 kOe. The spontaneous magnetic moments determined by extrapolating the linear part of $M(H)$ at $T = 2$ K to $H = 0$ before and after the metamagnetic transitions are 2.1 and 3.6 μ_B/f.u., respectively; both are significantly lower than the theoretical 5.52 μ_B for 0.6Pr+0.4Er, suggesting noncollinearity even in the 140 kOe magnetic field. At least four main transitions are seen in dM/dH data [inset f, Fig. 4(a)]. Both the hysteresis and the critical fields for the metamagnetic transitions decrease with increasing temperatures [Fig. 4(b) and inset Fig. 4(c)]. At $T = 24$ K, the $M(H)$ curve shows FIM behavior [Fig. 4(c)]. This is consistent with the $M(T)$ data of Figs. 1 and 2.

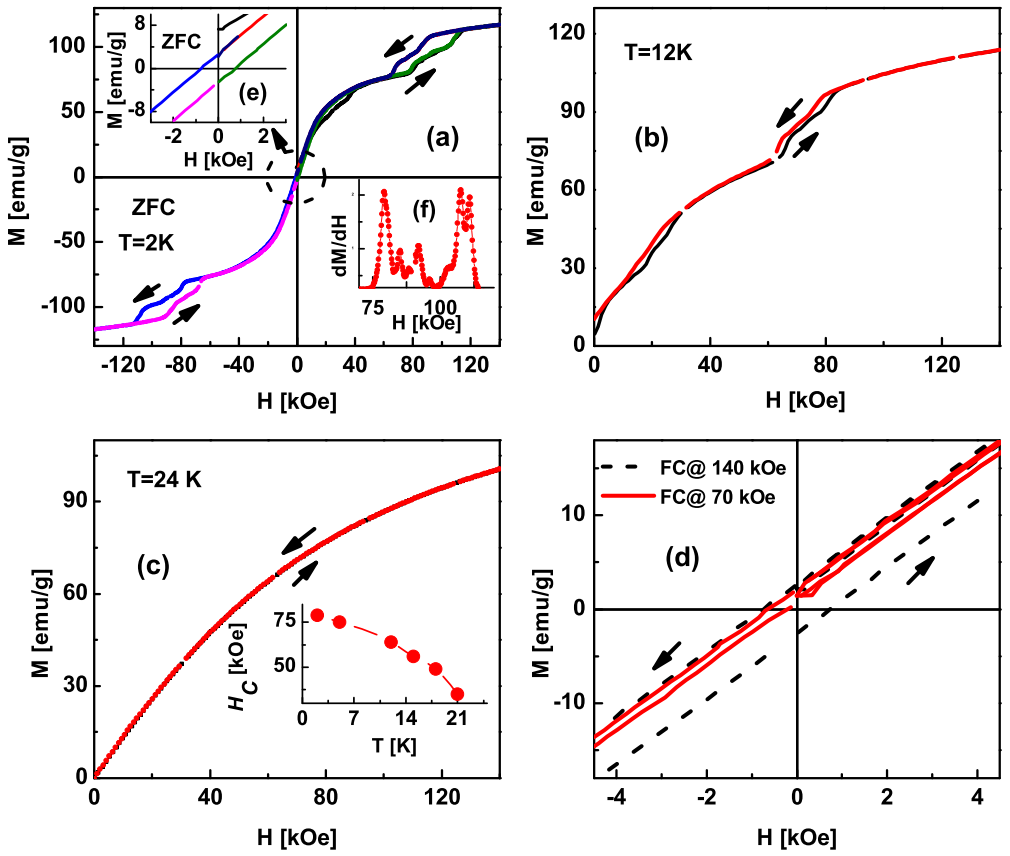

FIG. 4. (Color online) Zero field cooled magnetization of $Pr_{0.6}Er_{0.4}Al_2$ measured as a function of magnetic field at $T = 2$ K (a), $T = 12$ K (b), and $T = 24$ K (c). The insets (e) and (f) in (a) show details of low-field hysteresis loops, and derivative of $M(H)$ for magnetic fields -3 kOe $\rightarrow$ 3 kOe and 75 $\rightarrow$ 115 kOe at $T = 2$ K, respectively. The inset in (c) shows critical fields for which metamagnetic transition starts as a function of temperature. (d) Field-cooled (FC) hysteresis loops of $Pr_{0.6}Er_{0.4}Al_2$ at $T = 2$ K after the sample is cooled down from 300 K in magnetic fields of 140 kOe (dashed lines) and 70 kOe (solid lines). Only parts of the hysteresis loops from $-4.5 \rightarrow 4.5$ kOe are shown in (d) for clarity.

The ZFC $M(H)$ hysteresis loops are symmetrical [inset e, Fig. 4(a)]. However, when the sample is cooled from the PM state in positive magnetic fields ($H \geqslant 200$ Oe), the hysteresis loops are displaced toward the negative values of the field axis. The displacement does not disappear when cooling is done in a 70 kOe field [Fig. 4(d)]. EB, calculated as $H_{EB} = |H_1 + H_2|/2$, where H_1 and H_2 are respectively left and right cutoff fields of the $M = 0$ axis, is $H_{EB} \cong 440$ Oe for cooling in $H = 70$ kOe, which is significantly higher compared to that observed in other intermetallic compounds [31], and it is similar to that reported for $LaFeO_3$ nanoparticles [32]. However, after cooling in a much higher magnetic field of 140 kOe, the $M(H)$ loop becomes nearly symmetrical [Fig. 4(d), dashed line]; i.e., the exchange bias field is reduced to near zero due to the increased volume fraction of the field-induced FM phase (Fig. 1).

In contrast to thin films, where exchange interactions between FM and AFM layers are in the origin of EB, the different single-ion anisotropies of Pr and Er ions coupled with the opposite nearest-neighbor and next-nearest-neighbor exchange interactions (see below) affected by the magnetic field are the microscopic origin of the EB phenomenon in $Pr_{0.6}Er_{0.4}Al_2$. The anisotropic but antiparallel nearest-neighbor alignments of Pr and Er atoms may change to anisotropic but parallel alignments as a function of magnetic field, giving rise to the EB effects in this nonlayered system. A similar EB effect seen in bulk Mn_2PtGa supports this argument [10], where it was shown that FIM ordering is required to induce the exchange anisotropy for the ZFC EB.

Heat capacity, C_p, measured in various magnetic fields is shown in Fig. 5. C_P exhibits a typical behavior for second-order phase transformations, a λ-like peak at $T_C = 24$ K for $H = 0$ kOe [Fig. 5(a)]. Above 24 K, C_P gradually increases with temperature, and it reaches 72.2 J mol^{-1} K^{-1} at $T = 300$ K [Fig. 5(a)], which is close to the classical Dulong and Petit limit of the lattice heat capacity at constant volume $C_V = 74.83$ J mol^{-1} K^{-1} [33]. Compared to $PrAl_2$ [inset Fig. 5(a)], the peak value of C_p is significantly suppressed, and the peak itself shifts to lower temperature with the Er substitutions; the latter is expected, since $PrAl_2$ and $ErAl_2$ order ferromagnetically at ∼32.5 K and ∼14 K, respectively. The temperature at which the λ-type peak is observed in zero field C_p is in good agreement with the temperature at which a kink is observed in $M(T)$ data in 1 kOe (arrow in inset a, Fig. 2). The λ-like anomaly of C_P is preserved in magnetic fields of 10 and 20 kOe [Fig. 5(b)].

Upon a further increase of the field $30 \leqslant H \leqslant 70$ kOe, the observed C_p develops a sharp first-order-like peak shifted

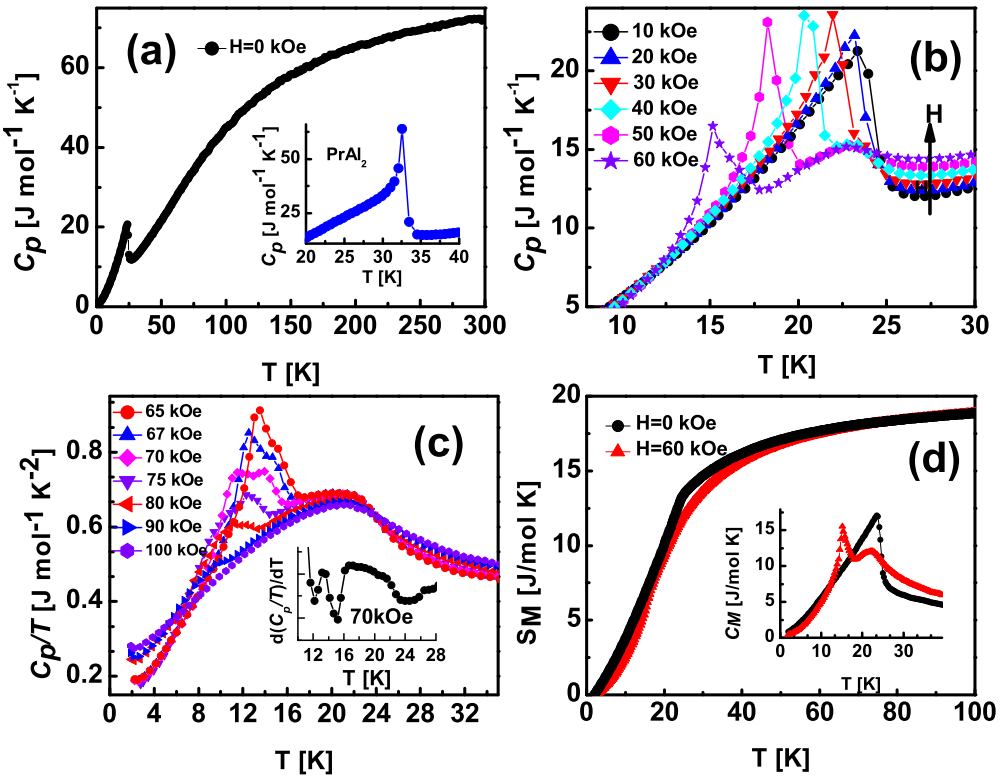

FIG. 5. (Color online) (a) Heat capacity C_p of $Pr_{0.6}Er_{0.4}Al_2$ measured in zero magnetic field. The inset shows the details of C_p for $PrAl_2$ near the phase transition. (b) C_p as a function of temperature shown in the vicinity of T_C for $10 \leqslant H \leqslant 60$ kOe. (c) C_p/T as a function of temperature for magnetic fields $65 \leqslant H \leqslant 100$ kOe. The inset in (c) shows $dC_p/T/dT$ in the vicinity of the phase transition for $H = 70$ kOe. (d) Magnetic entropy as a function of temperature for $H = 0$ and 60 kOe. Inset in (d) shows the magnetic contributions to the heat capacity (C_M) for $H = 0$ and 60 kOe.

to lower temperatures plus a higher-temperature broad peak [Fig. 5(b)], suggesting that $Pr_{0.6}Er_{0.4}Al_2$ undergoes at least two phase transitions, confirming the $M(T)$ measurements (Fig. 1). We note that even though the heat capacity anomaly at $H = 40$ kOe [Fig. 5(b)] appears relatively broad, this is the result of an overlap between the sharp first-order peak, which becomes more clear at 50 kOe and 60 kOe, and a broad second-order anomaly near 24 K. The temperature at which the steplike increase of magnetization is observed [Fig. 1(d)] corresponds to the temperature of the sharp first-order-like peak observed in C_p. Both FIM and FM phases coexist for $30 \leqslant H \leqslant 90$ kOe, and for $H \geqslant 100$ kOe, the compound exhibits only an FM to PM transition [Figs. 5(c) and 1(e)]. The well-developed thermal hysteresis between FCC and FCW $M(T)$ at $H = 70$ kOe below $T < 20$ K [Fig. 2(d)] confirms the field-induced first-order phase transitions observed in C_p measurements (Fig. 5). Figure 5(d) shows magnetic entropy as a function of temperature estimated by subtracting the prorated heat capacities of nonmagnetic $LaAl_2$ and $LuAl_2$ from the heat capacity of $Pr_{0.6}Er_{0.4}Al_2$, as described in Ref. [34]. Upon the application of a magnetic field, the magnetic contribution to the heat capacity (C_M) clearly shows two anomalies: a low-temperature sharp peak followed by a broad high-temperature anomaly [Fig. 5(d) inset]. The magnetic entropy above T_C ($T = 100$ K) is 19 J mol^{-1} K^{-1}, which is ~93% of the theoretical value, S_M (theory) $= R\ln(2J + 1) = 20.5$ J mol^{-1} K^{-1}.

Figure 6 shows the temperature-magnetic field phase diagram obtained from heat capacity data. The FIM transition temperature decreases rapidly with increasing external magnetic field from ~25 K at $H = 0$ kOe to ~9 K at $H = 80$ kOe, and the FIM phase is no longer observed at $H = 100$ kOe. The field-induced FM transition temperature increases slowly

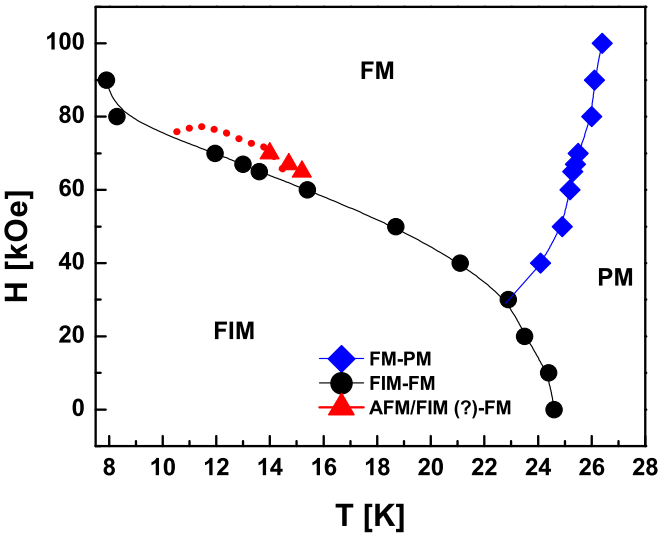

FIG. 6. (Color online) Temperature–magnetic field phase diagram of $Pr_{0.6}Er_{0.4}Al_2$.

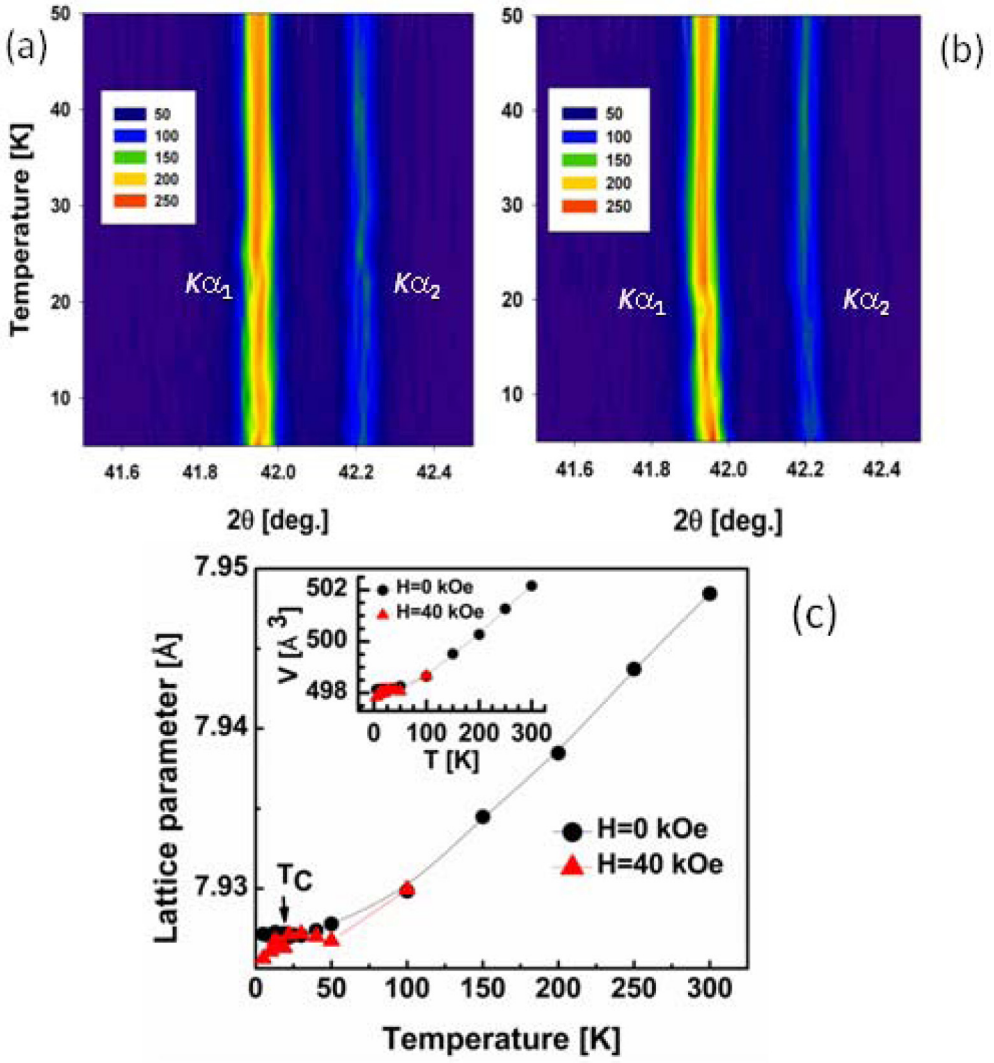

FIG. 7. (Color online) The intensity contour map of the x-ray diffraction patterns of $Pr_{0.6}Er_{0.4}Al_2$ in the vicinity of (008) Bragg peak measured in (a) $H = 0$ kOe and (b) $H = 40$ kOe. (c) The temperature dependencies of the lattice parameter in a 0 and 40 kOe magnetic field. The inset in (c) shows the phase volume as a function of temperature at $H = 0$ and 40 kOe.

with field. In addition to these phase transformations, at intermediate magnetic fields $65 \leqslant H \leqslant 70$ kOe, the compound undergoes an additional FIM (or AFM)-like transition [see Fig. 5(c)]. This may be due to a change from one noncollinear FIM (or AFM) structure to another FIM (or AFM) structure before transforming to the FM structure.

Figure 7 shows the intensity contour map of the x-ray powder diffraction patterns and temperature dependence of the lattice parameter of $Pr_{0.6}Er_{0.4}Al_2$ in 0 and 40 kOe magnetic fields. Unlike the cubic to tetragonal distortion in $PrAl_2$ [13], $Pr_{0.6}Er_{0.4}Al_2$ retains its cubic $MgCu_2$ Laves phase-type structure in all measured fields and temperatures, and it rules out the possibility of structural distortions associated with a sharp peak in the heat capacity at $H \leqslant 40$ kOe and $T < 22$ K [Fig. 5(b)]. At $H = 0$ kOe, the unit cell volume changes continuously, suggesting that the transition at T_C is a second-order transformation, which is consistent with the heat capacity data shown in Fig. 5(a). However, both the unit cell dimensions and volume change become anomalous at $H = 40$ kOe, i.e., as the sample passes through the first-order transition in T-H coordinate space (see magnetization and heat capacity in Figs. 1 and 5).

Consistent with experiment, the total energy of FIM $Pr_{0.625}Er_{0.375}Al_2$ is lower by 112 meV/cell compared to the FM configuration. The calculated magnetic moments are 2.36 μ_B for Pr in FM $PrAl_2$ and 8.88 μ_B for Er in FM $ErAl_2$, whereas the average moments are 1.86 μ_B/R and 4.80 μ_B/R in FIM and FM $Pr_{0.625}Er_{0.375}Al_2$, respectively. Local spin density approximation with the Hubbard U (LSDA+U) reveals CF split spin up/down $4f$ states [Fig. 8(a)], which form a gap across the Fermi level (the CF excitation gap) associated with transitions between different $4f$ multiplets [35]. The gap itself is dependent on the electron-electron correlations, which results in the change of the magnetic states via the admixing of the CF split states [36] just above and below the Fermi level. Further, the degeneracy of the multiplets may be lifted by Zeeman interactions [37] as a result of applying a magnetic field that gives additional magnetic excitations associated either with the fluctuations of the moments or with multiple magnetic transitions [35], which are indeed observed experimentally.

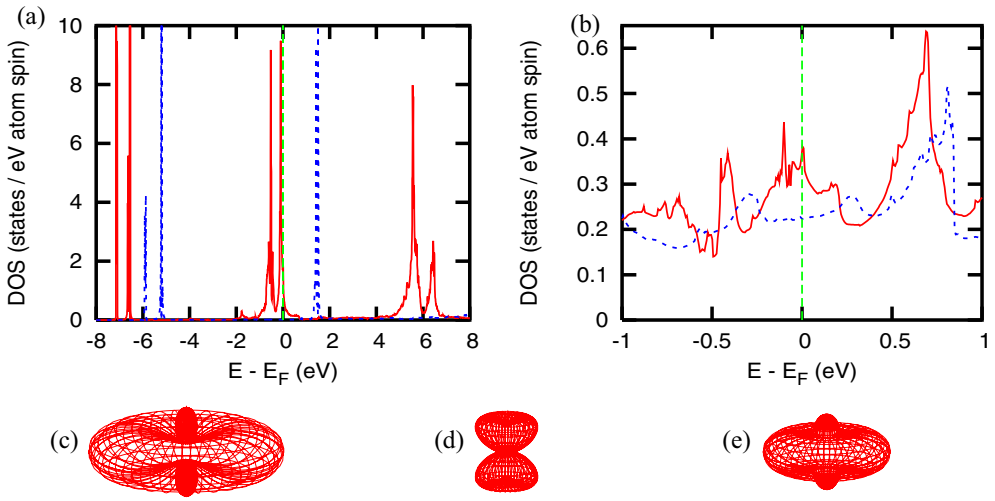

FIG. 8. (Color online) (a) $4f$ and (b) $5d$ densities of states of $Pr_{0.625}Er_{0.375}Al_2$. The CF split spin up/down $4f$ bands form a gap across the Fermi level. (c) The $4f$ charge densities of Pr in $PrAl_2$, (d) Er in $ErAl_2$, and (e) $Pr_{0.625}Er_{0.375}Al_2$ from point charge model [38,39] calculations including quadrupolar (Q_2/a_o^2) and octupolar (Q_4/a_o^4) moments.

Figure 8(b) shows spin-polarized $5d$ density of states (DOS) due to the indirect $4f$-$4f$ exchange interactions. The $5d$ DOS [Fig. 8(b)] is modified across the Fermi level due to the hybridization of CF split $4f$ and conduction $5d$ states. Hence, the indirect $4f$-$4f$ exchange interactions in $Pr_{0.6}Er_{0.4}Al_2$ are controlled by CF split $4f$ states and their hybridization with $5d$ states.

Figures 8(c) and 8(d) show the $4f$ charge densities of $PrAl_2$ and $ErAl_2$, respectively, calculated by using a point charge model [38,39] including quadrupolar and octupolar moment contributions. When differently shaped $4f$ charge densities of Pr [Fig. 8(c)] and Er [Fig. 8(d)] are mixed, the resultant $4f$ charge density of $Pr_{0.625}Er_{0.375}Al_2$ [Fig. 8(e)] tends to be spherical. The instability that results from changing the signs of both the higher-order moment contributions and the anisotropy constant [40] near the 0.6Pr/0.4Er concentration leads to multiple magnetic transitions, which are observed experimentally.

Every R atom in $Pr_{0.6}Er_{0.4}Al_2$ is surrounded by 4, 12, 12, and 6 nearest-neighbor through fourth-nearest-neighbor $R(R')$ atoms at $\delta_{R-R} = a\sqrt{3}/4 \cong 3.4$ Å, $a/\sqrt{2} \cong 5.6$ Å, $a\sqrt{11}/4 \cong 6.6$ Å, and $a \cong 7.9$ Å, respectively. The probability to find a Pr atom in any of these locations is 60% (40% for the Er atom). The differences in the magnetic ordering in this mixed-lanthanide system may be visualized using the effective magnetic surface potential (EMSP, or k-space potential), $J(h)$. The latter can be expanded using a Fourier series limited to the first few near-neighbor magnetic exchange interaction parameters, $j(s)$, as $J(h) = \sum_s j(s)Y^{(s)}(h)$. Here, $Y^{(s)}(h)$, given in Ref. [41] for an arbitrary coordination shell, s, of the face centered cubic structure, has been modified for the $MgCu_2$-type Laves phase structure.

Figures 9(a) and 9(b) illustrate EMSPs in $Pr_{0.625}Er_{0.375}Al_2$ calculated assuming positive [Fig. 9(a)] or negative [Fig. 9(b)] exchange interactions up to the fourth coordination shell. As expected, the maxima and minima are opposite. From DFT, $j(s) < 0$ for $s = 1$, 3, and 4, but $j(s) > 0$ for $s = 2$. Second-nearest-neighbor exchange interactions [$j(2) = 12.5$ meV] are slightly weaker than the nearest-neighbor ones [$j(1) = -13.6$ meV]; $j(3)$ and $j(4)$ are reduced by approximately one and two orders of magnitude, respectively, and therefore are nearly negligible. The EMSP constructed using $j(1)$ through $j(4)$ from DFT depicted in Fig. 9(c) shows the development of peaks at k-points corresponding to all $j(s) > 0$, while

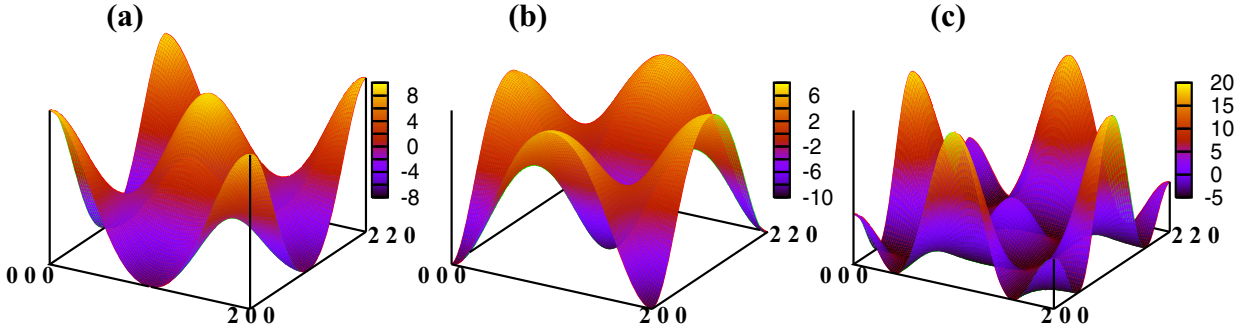

FIG. 9. (Color online) The magnetic surface potentials of $Pr_{0.625}Er_{0.375}Al_2$ assuming (a) $j(s) > 0$ for $s = 1$, 2, 3, and 4, (b) $j(s) < 0$ for $s = 1$, 2, 3, and 4, and (c) $j(s)$ predicted from DFT for $s = 1$, 2, 3, and 4 (c). The z-axis is the magnetic surface potential axis in mRyd per atom (1 mRyd = 13.6 meV).

simultaneously shifting the minima from the $j(s) < 0$ structure away from the ends of k-vectors. The magnetic structure observed in $H = 0$ may, therefore, become unstable, leading to the Griffiths phase behavior in low magnetic fields and multiple metamagnetic transitions when the magnetic field is increased.

IV. CONCLUSIONS

In conclusion, we report coexistence of FM and FIM, and metamagnetism in the presence of a magnetic field in $Pr_{0.6}Er_{0.4}Al_2$. Unexpectedly, the Griffiths phase behavior is observed even at $H = 1$ kOe. The compound exhibits numerous phase transitions, including first-order FIM to FM and second-order FM to PM transitions at $30 \leqslant H \leqslant 80$ kOe. A large EB effect is observed when the sample is cooled down at a magnetic field of 70 kOe from the PM state; however, $M(H)$ becomes isotropic and EB is zero when the sample is cooled down at 140 kOe. The FIM ground state has been determined by neutron diffraction and supported by DFT. The theoretical calculations indicate that the observed physical behaviors are due to the opposite first- and second-nearest-neighbor interactions, crystal field splitting, and magnetic instability related to effectively spherical $4f$ charge density distribution, which is intermediate between the oblate (Pr) and prolate (Er) $4f$ charge densities of the constituent lanthanides.

ACKNOWLEDGMENTS

This work was supported by the U.S. Department of Energy (DOE), Office of Science, Basic Energy Sciences, Materials Science and Engineering Division. The research was performed at the Ames Laboratory, which is operated for the U.S. DOE by Iowa State University under Contract No. DE-AC02-07CH11358. Research at the Oak Ridge National Laboratory High Flux Isotope Reactor is sponsored by the Scientific User Facilities Division, Office of Basic Energy Sciences, U.S. DOE.

[1] A. H. Castro Neto, G. Castilla, and B. A. Jones, Phys. Rev. Lett. **81**, 3531 (1998).
[2] Y. Tokura, H. Kuwahara, Y. Moritomo, Y. Tomioka, and A. Asamitsu, Phys. Rev. Lett. **76**, 3184 (1996).
[3] C. Krey, S. Legl, S. R. Dunsiger, M. Meven, J. S. Gardner, J. M. Roper, and C. Pfleiderer, Phys. Rev. Lett. **108**, 257204 (2012).
[4] C. M. Bonilla, N. Marcano, J. Herrero-Albillos, A. Maisuradze, L. M. García, and F. Bartolomé, Phys. Rev. B **84**, 184425 (2011).
[5] C. Magen, P. A. Algarabel, L. Morellon, J. P. Araújo, C. Ritter, M. R. Ibarra, A. M. Pereira, and J. B. Sousa, Phys. Rev. Lett. **96**, 167201 (2006).
[6] Robert B. Griffiths, Phys. Rev. Lett. **23**, 17 (1969).
[7] M. B. Salamon, P. Lin, and S. H. Chun, Phys. Rev. Lett. **88**, 197203 (2002).
[8] S. A. Wolf, D. D. Awschalom, R. A. Buhrman, J. M. Daughton, S. von Molnár, M. L. Roukes, A. Y. Chtchelkanova, and D. M. Treger, Science **294**, 1488 (2001).
[9] S. Brück, J. Sort, V. Baltz, S. Suriñach, J. S. Muñoz, B. Dieny, M. D. Baró, and J. Nogués, Adv. Mater. **17**, 2978 (2005).
[10] A. K. Nayak, M. Nicklas, S. Chadov, C. Shekhar, Y. Skourski, J. Winterlik, and C. Felser, Phys. Rev. Lett. **110**, 127204 (2013).
[11] B. M. Wang, Y. Liu, P. Ren, B. Xia, K. B. Ruan, J. B. Yi, J. Ding, X. G. Li, and L. Wang, Phys. Rev. Lett. **106**, 077203 (2011).
[12] H. G. Purwins and A. Leson, Adv. Phys. **39**, 309 (1990).
[13] A. K. Pathak, D. Paudyal, Ya. Mudryk, K. A. Gschneidner, Jr., and V. K. Pecharsky, Phys. Rev. Lett. **110**, 186405 (2013).
[14] A. L. Lima, K. A. Gschneidner, Jr., V. K. Pecharsky, and A. O. Pecharsky, Phys. Rev. B **68**, 134409 (2003).
[15] W. M. Swift and W. E. Wallace, J. Phys. Chem. Solids **29**, 2053 (1968).
[16] A. Magnus, G. Carvalho, F. Garcia, V. S. R. de Sousa, P. J. von Ranke, D. L. Rocco, G. D. Loula, E. J. de Carvalho, A. A. Coelho, L. M. da Silva, and F. C. G. Gandra, J. Magn. Magn. Mater. **321**, 3014 (2009).
[17] P. D. Kulkarni, A. Thamizhavel, V. C. Rakhecha, A. K. Nigam, P. L. Paulose, S. Ramakrishnan, and A. K. Grover, Europhys. Lett. **86**, 47003 (2009).
[18] Materials Preparation Center, Ames Laboratory of U.S. DOE, Ames, Iowa, USA, www.mpc.ameslab.gov
[19] A. P. Holm, V. K. Pecharsky, K. A. Gschneidner, Jr., R. Rink, and M. Jirmanus, Rev. Sci. Instrum. **75**, 1081 (2004).
[20] B. Hunter, Rietica—A Visual Rietveld Program, International Union of Crystallography Commission on Powder Diffraction Newsletter No. 20, (Summer, 1998), http://www.rietica.org
[21] V. K. Pecharsky, J. O. Moorman, and K. A. Gschneidner, Jr., Rev. Sci. Instrum. **68**, 4196 (1997).
[22] V. O. Garlea, B. C. Chakoumakos, S. A. Moore, G. B. Taylor, T. Chae, R. G. Maples, R. A. Riedel, G. W. Lynn, and D. L. Selby, Appl. Phys. A **99**, 531 (2010).
[23] J. Rodriguez-Carvajal, Physica B **192**, 55 (1993). The Rietveld refinement program is available at http://www.ill.eu/sites/fullprof/
[24] V. I. Anisimov, F. Aryasetiawan, and A. I. Lichtenstein, J. Phys.: Condens. Matter **9**, 767 (1997).
[25] O. K. Andersen and O. Jepsen, Phys. Rev. Lett. **53**, 2571 (1984).
[26] P. Blaha, K. Schwarz, G. Madsen, D. Kvasnicka, and J. Luitz, *WIEN2k, An Augmented Plane Wave + Local Orbitals Program for Calculating Crystal Properties* (Karlheinz Schwarz, Techn. Universität Wien, Austria, 2001).
[27] S. Guo, D. P. Young, R. T. Macaluso, D. A. Browne, N. L. Henderson, J. Y. Chan, L. L. Henry, and J. F. DiTusa, Phys. Rev. Lett. **100**, 017209 (2008).
[28] R. Nirmala, Ya. Mudryk, V. K. Pecharsky, and K. A. Gschneidner, Jr., Phys. Rev. B **76**, 014407 (2007).
[29] P. D. Kulkarni, U. V. Vaidya, V. C. Rakhecha, A. Thamizhavel, S. K. Dhar, A. K. Nigam, S. Ramakrishnan, and A. K. Grover, Phys. Rev. B **78**, 064426 (2008).
[30] N. Nereson, C. Olsen, and G. Arnold, J. Appl. Phys. **39**, 4605 (1968).
[31] M. Khan, I. Dubenko, S. Stadler, and N. Ali, Appl. Phys. Lett. **91**, 072510 (2007).
[32] H. Ahmadvand, H. Salamati, P. Kameli, A. Poddar, M. Acet, and K. Zakeri, J. Phys. D: Appl. Phys. **43**, 245002 (2010).

[33] C. Kittel, *Introduction to Solid State Physics*, 8th ed. (Wiley, New York, 2005).
[34] M. Khan, K. A. Gschneidner, Jr., and V. K. Pecharsky, Phys. Rev. B **80**, 224408 (2009).
[35] J. Jensen and A. Mackintosh, *Rare Earth Magnetism* (Clarendon Press, Oxford, 1991), p. 312.
[36] P. Bak, Danish Atomic Energy Commission Research Establishment Risø, Risø Report No. 312 (1974).
[37] T. Balcerzak, Phys. Status Solidi C **3**, 212 (2006).
[38] A. J. Freeman and R. E. Watson, Phys. Rev. **127**, 2058 (1962).
[39] P. Fulde, in *Handbook on the Physics and Chemistry of Rare Earths*, edited by K. A. Gschneidner, Jr. and L. Eyring, Vol. 2 (North-Holland, New York, 1979).
[40] D. Paudyal, A. K. Pathak, V. K. Pecharsky, and K. A. Gschneidner, Jr., J. Phys.: Condens. Matter **25**, 396002 (2013).
[41] D. de Fontaine, *Solid State Physics*, edited by H. Ehrenreich, F. Seitz, and D. Turnbull (Academic Press, New York, 1979), Vol. 34, p. 73.